

This is a repository copy of *Particle acceleration during merging-compression plasma start-up in the Mega Amp Spherical Tokamak*.

White Rose Research Online URL for this paper:

<https://eprints.whiterose.ac.uk/123753/>

Version: Submitted Version

Article:

McClements, K G, Allen, Joe Oliver, Chapman, S. et al. (6 more authors) (2017) Particle acceleration during merging-compression plasma start-up in the Mega Amp Spherical Tokamak. *Plasma Physics and Controlled Fusion*. ISSN 1361-6587

<https://doi.org/10.1088/1361-6587/aa98fa>

Reuse

Items deposited in White Rose Research Online are protected by copyright, with all rights reserved unless indicated otherwise. They may be downloaded and/or printed for private study, or other acts as permitted by national copyright laws. The publisher or other rights holders may allow further reproduction and re-use of the full text version. This is indicated by the licence information on the White Rose Research Online record for the item.

Takedown

If you consider content in White Rose Research Online to be in breach of UK law, please notify us by emailing eprints@whiterose.ac.uk including the URL of the record and the reason for the withdrawal request.

Particle acceleration during merging-compression plasma start-up in the Mega Amp Spherical Tokamak

K.G. McClements¹, J. Allen², S.C. Chapman³, R.O. Dendy^{1,3}, S.W.A. Irvine³, O. Marshall², D. Robb⁴, M. Turnyanskiy¹, R.G.L. Vann²

¹ CCFE, Culham Science Centre, Abingdon, Oxfordshire OX14 3DB, UK

² Dept of Physics, University of York, Heslington, York, YO10 5DD, UK

⁴ Dept of Physics, University of Warwick, Coventry CV4 7AL, UK

³ Dept of Physics and Astronomy, University of Glasgow, Glasgow, G12 8QQ, UK

Abstract

The merging-compression method of plasma start-up in the Mega Amp Spherical Tokamak (MAST) involved the creation of two plasma tori with parallel currents, which merged at the vacuum vessel midplane due to their mutual attraction. Magnetic reconnection occurred in this process causing strong heating of both ions and electrons on millisecond timescales, and resulting in a plasma equilibrium with a single set of closed magnetic flux surfaces. The merging process also resulted in the prompt acceleration of substantial numbers of ions and electrons to highly suprathermal energies. Accelerated field-aligned ions (deuterons and protons) were detected using a neutral particle analyser at energies up to about 20 keV during merging in early MAST pulses, while nonthermal electrons have been detected indirectly in more recent pulses through microwave bursts. However no increase in soft X-ray emission was observed until later in the merging phase, by which time strong electron heating had been detected through Thomson scattering measurements. A test-particle code CUEBIT is used to model ion acceleration in the presence of an inductive toroidal electric field with a prescribed spatial profile and temporal evolution based on Hall-MHD simulations of the merging process. The magnetic field used in the modelling includes a poloidal component consistent with this electric field. The simulations yield particle distributions with properties similar to those observed experimentally, including the acceleration of protons to higher energies than deuterons, as expected from simple estimates, and the strong field alignment of the fast ion pitch angle distributions. Particle-in-cell modelling of a plasma containing a dilute field-aligned suprathermal electron component suggests that at least some of the microwave bursts can be attributed to the anomalous Doppler instability driven by anisotropic fast electrons, which do not produce measurable enhancements in soft X-ray emission either because they have energies below about 1 keV or because the nonthermal bremsstrahlung emissivity during this phase of the pulse is below the detection threshold. There is no evidence of runaway electron acceleration during merging in MAST, possibly due to the presence of three-dimensional field perturbations.

1 Introduction

Toroidal plasmas in the Mega Amp Spherical Tokamak (MAST) were routinely started by forcing two separate plasma tori to merge in the vessel midplane, causing magnetic reconnection to occur [1]. MAST was equipped with a wide range of excellent diagnostics, and therefore this start-up scheme provided a valuable opportunity to study experimentally the physics of magnetic reconnection in the high energy density conditions of a tokamak plasma, but without some of the complications of other types of tokamak reconnection events, such as sawteeth. In particular, to a good approximation, reconnection during merging in MAST can be regarded as an axisymmetric (two-dimensional) process, greatly facilitating both the interpretation of experimental data and the modelling of these data. Tanabe and co-workers [1] have used Thomson scattering and carbon line radiation measurements to produce two-dimensional maps of electron and ion heating during merging, demonstrating that electrons were heated initially at the merging point of the two original tori, while ion heating was attributed to viscous dissipation of outflows arising from the reconnection process. Later, electrons were heated in the outflow regions and ions at the merging point, due to electron-ion collisional equilibration. Higher electron and ion temperatures were recorded at the merging point when the toroidal component of the magnetic field was increased, as expected from Braginskii-type scaling of cross-field collisional transport [2]. Axisymmetric magnetohydrodynamic (MHD) and Hall-MHD modelling of merging-reconnection in MAST has produced results that are broadly consistent with experimental measurements, and provided useful information on the likely evolution of the magnetic field during this process [3].

In this paper we focus on another common consequence of magnetic reconnection in weakly collisional plasmas, the generation of suprathermal particles. This study is motivated in part by the fact that particle acceleration has previously been found to be correlated with other types of reconnection events in MAST [4]. The production of energetic particles in tokamak plasmas through processes other than fusion reactions, neutral beam injection or radio-frequency heating is generally considered to be undesirable, since the presence of these particles is liable to cause non-classical losses of energy from the plasma or damage to plasma-facing solid surfaces, and for this reason it is important to understand their origin. A second motivation arises from the fact that the dimensionless parameters of plasmas during merging in MAST are similar to those in the flaring solar corona [5], where it is well-established that reconnection causes the production of large numbers of nonthermal electrons and ions, detected primarily via hard X-ray and γ -ray emission [6]. On this basis it is reasonable to suppose that useful insights into the physics of particle acceleration in flares might be gained by studying this process in MAST, where measurements can be carried out in close proximity to the plasma rather than at a distance of 150 million km.

Neutral particle analyser (NPA) measurements of fast ion production during merging in MAST were first reported in Ref [5]. In section 2 we present further details of these NPA measurements, and also report on observations of microwave bursts which provide strong evidence of nonthermal electron production during merging. Modelling of ion acceleration, based on an analytically-prescribed time-varying magnetic flux, is

presented in section 3, while results from a particle-in-cell simulation of a plasma containing anisotropic fast electrons are used in section 4 to interpret the microwave burst measurements. Conclusions and a discussion of the possible role of three-dimensional effects are presented in section 5.

2 Merging-compression plasma start-up in MAST

Detailed descriptions of merging-compression plasma start-up in MAST can be found in Refs [1, 3]. In summary, plasma rings with parallel toroidal currents were formed around coils located above and below the vessel midplane, subsequently detaching and merging in the midplane due to their mutual attraction. A change of magnetic field line topology (i.e. reconnection) from two tori to a single torus with nested magnetic surfaces typically occurred around 4-5 ms after the start of the pulse. In the two subsections below we describe NPA and microwave measurements obtained during this merging process.

2.1 Neutral particle analyser measurements of fast ions

The MAST NPA measured fluxes of deuterium and hydrogen atoms resulting from charge exchange between plasma ions and neutrals, with 39 energy channels for each species [7]. As shown in figure 1, the NPA line-of-sight could be changed from pulse to pulse such that its minimum major radius R_{NPA} (i.e. the major radius at which the line-of-sight was tangential to the toroidal direction) ranged from about 1.33 m for views in the clockwise direction (as seen from above) to about 0.46 m for views in the anti-clockwise direction; in the latter case, we assign a negative value to R_{NPA} . In normal MAST operation the plasma current was anti-clockwise while the toroidal field was clockwise, and therefore fast ions moving in the co-current direction could be detected as neutrals by the NPA if R_{NPA} was positive and equal to the major radius of the ion when it was neutralised (the ion velocity being essentially unaffected by the charge exchange process).

As first reported in Ref [5], bursts of fast deuterons and protons were recorded across a wide range of energies by the NPA during the merging phase of MAST pulses, prior to the start of neutral beam injection. The dominant ion species in these plasmas was deuterium, but some hydrogen was also present, together with heavier impurity species. Figure 2 shows particle energy spectra obtained in a pulse with R_{NPA} set to its default value of 0.7 m. These were obtained by integrating the NPA fluxes over a period from 3-9 ms into the pulse, covering the entire merging phase. The energy-dependence of the charge exchange cross-section was taken into account, and therefore the spectra provide a true measure of the ion energy distributions (rather than the distributions of charge-exchanged neutrals). Thus, a Maxwellian ion distribution would appear as a straight line in a log-linear plot of the type shown in figure 2. In common with the spectra shown in Ref [5], it can be seen that protons were recorded at somewhat higher maximum energies than deuterons, and there was a deficit of protons in the lowest energy channel for this species, 5.2 keV (the apparent absence of protons at energies

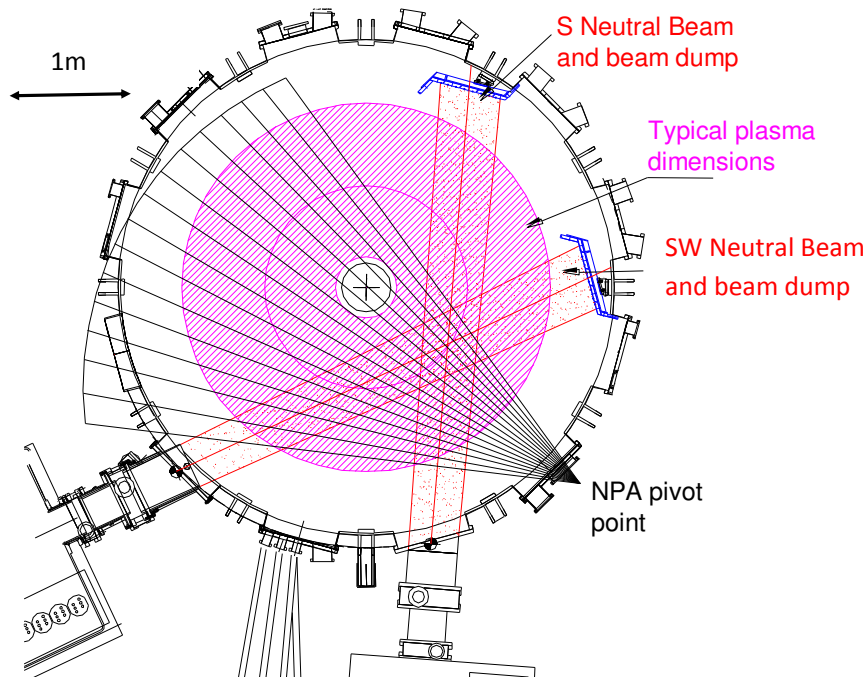


Figure 1: Layout of the MAST NPA system and neutral beams, as seen from above. The black lines indicate the possible NPA lines-of-sight: R_{NPA} is the shortest distance between one of these lines and the centre of the torus. Note that the neutral beams were not used during the merging-compression phase of MAST pulses.

below 5.2 keV is an artefact arising from the low-energy cutoff in the NPA).

It is important to note that the fall-off in the deuterium spectrum at energies above 4 keV cannot be attributed to the finite temperature of the bulk deuterium population. Thomson scattering measurements show that the electron temperature at the end of the merging phase in this pulse peaked at less than 200 eV, and direct measurements of ion temperature during the merging phases of more recent MAST pulses have yielded similar values [1]. In contrast, the deuterium spectrum in the energy range from 4-13 keV in figure 2 corresponds to an equivalent temperature of about 2.9 keV, which is considerably higher than the peak bulk ion temperatures measured during the flat-top phase of MAST plasmas with strong neutral beam heating (see e.g. figure 4 in [8]). It is thus clear that both the deuterium and hydrogen spectra shown in figure 2 were produced predominantly by suprathermal ions. However, fitting a straight line to the two lowest energy deuterium points in this figure, we obtain a temperature of about 200 eV, which is a realistic value for the bulk ion population.

In the case of the spectra shown in figure 2 R_{NPA} was comparable to major radii at which strong, localised electron heating was observed during merging [1], and it is reasonable to identify these locations with current sheets formed by the merging plasma rings, since strong Ohmic heating of the electrons is expected to occur there [3]. The magnetic field in MAST, as in all tokamaks, was predominantly toroidal. Thus, if we make the reasonable assumption that the fast ions recorded by the NPA during merging

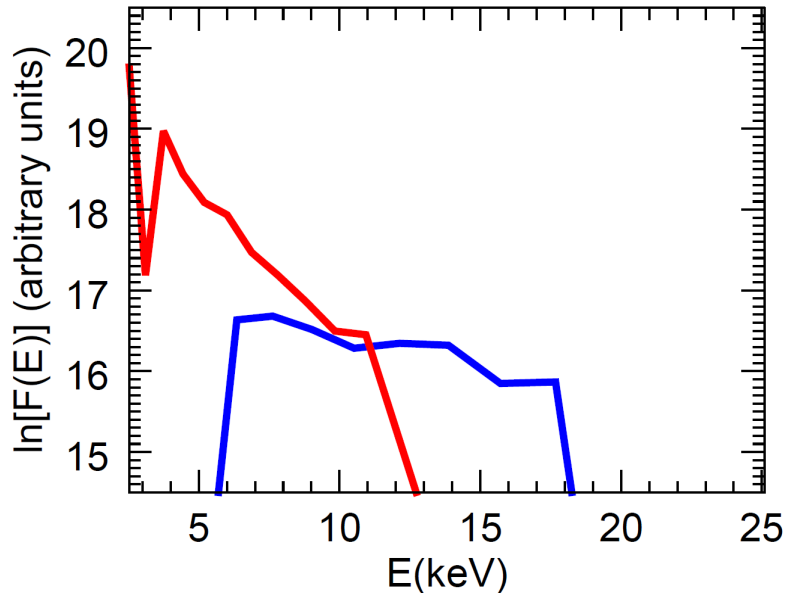


Figure 2: Deuterium (red) and hydrogen (blue) energy spectra recorded by the MAST NPA during the merging phase of pulse 9153.

reconnection originated from the current sheet region, where large parallel electric fields would be expected to occur, it follows that R_{NPA} can be regarded as a proxy for the fast ion pitch angle, with $R_{\text{NPA}} = 0.7$ m corresponding to pitch angles close to zero. By comparing NPA measurements in similar shots with different R_{NPA} it is thus possible to obtain information on the fast ion pitch angle distributions. Figure 3 shows the temporal evolution of the NPA flux in one particular hydrogen channel (16 keV) for shots with $R_{\text{NPA}} = 0.7$ m (black curve, pulse 9153) and -0.46 m (red curve, pulse 9161). The peak flux is much higher in the former case than the latter, suggesting that the fast ion distribution is strongly aligned with the magnetic field. Particle fluxes in this channel similar to those of pulse 9161 were recorded in pulses with $R_{\text{NPA}} = 0$ m and 0.46 m, while no neutrals were detected during the merging phases of pulses with $R_{\text{NPA}} = 1.23$ m and 1.33 m. These null results clearly indicate that none of the fast ions were located at major radii lying far outboard of the merging point. Similar results were obtained for other hydrogen channels of the NPA, and for deuterium channels.

Taking the inferred strong anisotropy of the accelerated fast ions into account, and assuming that the fluxes in the two lowest energy deuterium channels in figure 2 can be attributed to the bulk ion population, as suggested above, we estimate that the accelerated ion fraction during merging in this pulse was more than 10%. It should be noted that such estimates are very approximate [5], but nevertheless it appears that in some pulses a large fraction of the available ion population was energised by the merging-reconnection process.

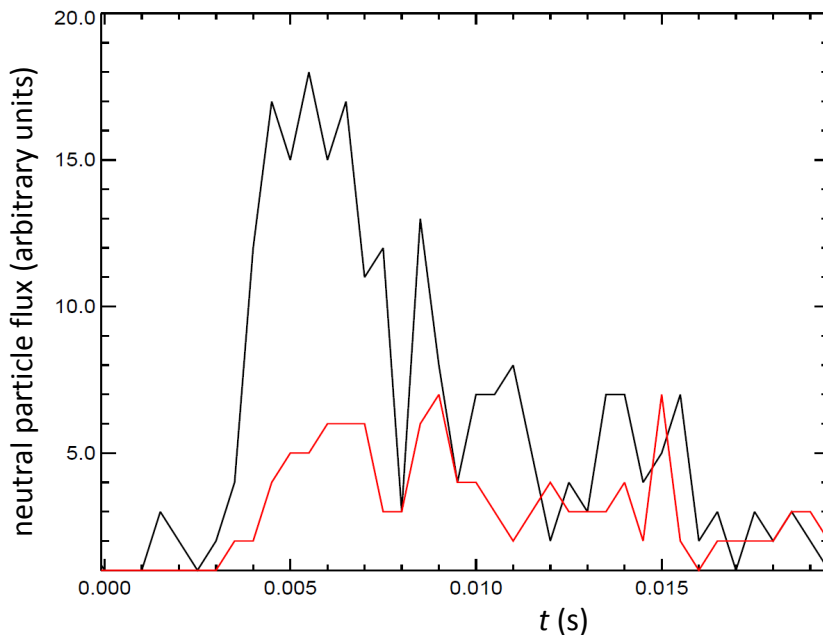


Figure 3: Neutral particle fluxes of 16 keV protons versus time in MAST pulses 9153 with $R_{\text{NPA}} = 0.7$ m (black) and 9161 with $R_{\text{NPA}} = -0.46$ m (red).

2.2 Microwave bursts

In the most recent MAST campaigns a microwave diagnostic known as SAMI (Synthetic Aperture Microwave Imaging) [9] was used to detect emission in the electron cyclotron frequency range (10 – 35 GHz). SAMI detects emission in fifteen different frequency channels sequentially, with $8 \mu\text{s}$ of data acquisition per channel and a total sweep time over all channels of $160 \mu\text{s}$. Short-lived bursts of emission were detected using this instrument in many pulses during the merging phase, most frequently at about the same time in each pulse ($t \simeq 4 - 5$ ms) as fast ions were observed using the NPA in early MAST campaigns: an example is shown in figure 4. In this case the microwave intensity at the peak emission frequency, averaged over the $160 \mu\text{s}$ sweep time, was about 14 dB above the background (thermal) level, but instantaneous intensities of up to about 30 dB above the background were recorded in one of the SAMI channels. As shown in figure 4, the bursts are narrow-band, in this case peaking at a frequency of around 28 GHz. In this particular burst supra-thermal emission occurred in only three channels and was recorded in only one frequency sweep, which means that the burst duration could have been as short as $27 \mu\text{s}$. Thomson scattering measurements in this pulse show that the electron temperature profile immediately after the merging phase peaked at a major radius R of about 0.5 m. At this location the toroidal magnetic field was about 0.82 T, so that the local electron cyclotron frequency ν_{ce} was about 23 GHz. The electron density at $R = 0.5$ m just before the burst was about $2.5 \times 10^{18} \text{ m}^{-3}$, corresponding to an upper hybrid frequency $\nu_{\text{UH}} \equiv (\nu_{ce}^2 + \nu_{pe}^2)^{1/2} \simeq 27 \text{ GHz}$ (ν_{pe} being the electron plasma frequency), which is close to the burst frequency.

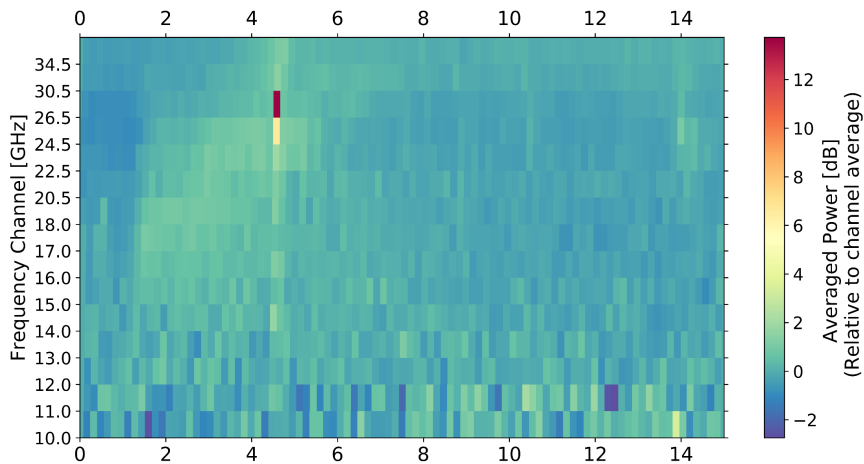


Figure 4: Dynamic spectrum of microwave emission recorded using SAMI during the first 10 ms of MAST pulse 28146.

A range of microwave burst frequencies is observed in different pulses. Figure 5 shows the frequency distribution of bursts with microwave intensity enhancements of at least 15 dB above the noise. The most common burst frequency is 24.5 GHz, but it can be seen that the distribution extends across almost the entire SAMI range (10–34.5 GHz). These pulses all had similar toroidal field values, and hence similar values of ν_{ce} at a given major radius.

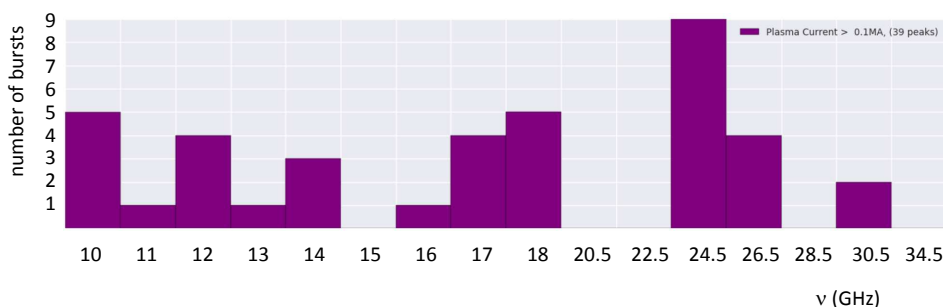


Figure 5: Frequency distribution of microwave bursts with intensity enhancements of at least 15 dB above the noise level. Note that the frequency scale is not exactly linear.

The high intensities and narrow bandwidths of these bursts strongly suggest the presence of suprathermal electrons in the plasma during the initial stages of the merging phase, but no clear evidence has yet been found for such electrons in either soft X-ray or Thomson scattering data. The soft X-ray cameras in MAST could detect photons with energies in the approximate range 1 – 30 keV, which means that electrons with energies above about 1 keV could in principle have been detected via bremsstrahlung, since for this process the energy of the emitted photon can be as high as that of the

electron producing it. Enhancements in soft X-ray emission from about $t \simeq 8$ ms onwards have been detected during some pulses in channels with lines-of-sight passing close to the plasma centre, but it is clear that these occurred due to bulk electron heating rather than electron acceleration, since strong electron heating at the merging point was observed in Thomson scattering profiles. With this point in mind, we will consider a possible interpretation of the microwave bursts in section 4.

3 Modelling of ion acceleration

3.1 Electric and magnetic fields

It was not possible to measure directly the electric or reconnecting magnetic fields in MAST during merging plasma start-up. However, as noted in section 1, a series of fluid simulations of this process, employing both MHD and Hall-MHD models [3], have provided useful insights into the likely evolution of the fields. All of these simulations were toroidally symmetric. In the more realistic Hall-MHD simulations, it was found that parallel electric fields of up to about 10 kV m^{-1} , persisting for about $1 \mu\text{s}$, were produced at the point where the plasma rings merged. In some of these simulations, magnetic islands were observed to form in the vicinity of the merging point (see figure 7 of Ref [3]).

In order to model particle acceleration resulting from this reconnection process, it is convenient to construct an analytical representation of the poloidal flux ψ , defined here such that the poloidal magnetic field \mathbf{B}_θ is equal to $\nabla\psi \times \nabla\varphi$, φ being toroidal angle in right-handed (R, φ, Z) cylindrical coordinates. The key feature of reconnection which needs to be encapsulated here is the generation of an inductive electric field from the annihilation of magnetic flux in the region where the plasma rings merge. A simple way of doing this is to use a time-dependent flux of the form

$$\psi(R, Z, t) = \psi_0 e^{-t^2/\tau^2} \exp \left[-\frac{(R - R_0)^2}{\delta R^2} - \frac{Z^2}{\delta Z^2} \right], \quad (1)$$

where ψ_0 , τ , R_0 , δR and δZ are constants whose values fix the magnitude, duration and spatial localisation of the reconnection-induced electric field and the associated poloidal magnetic field. At any given time, ψ is thus assumed to have elliptical contours in the (R, Z) plane, which are suggested by the magnetic islands observed in the Hall-MHD simulations of Stanier and co-workers [3].

The electric field corresponding to the above expression for ψ is given by

$$E_\varphi = -\frac{1}{R} \frac{\partial \psi}{\partial t} = \frac{2t}{R\tau^2} \psi_0 e^{-t^2/\tau^2} \exp \left[-\frac{(R - R_0)^2}{\delta R^2} - \frac{Z^2}{\delta Z^2} \right], \quad (2)$$

while the poloidal magnetic field has components

$$B_R = -\frac{1}{R} \frac{\partial \psi}{\partial Z} = \frac{2Z}{R\delta Z^2} \psi_0 e^{-t^2/\tau^2} \exp \left[-\frac{(R - R_0)^2}{\delta R^2} - \frac{Z^2}{\delta Z^2} \right], \quad (3)$$

and

$$B_Z = \frac{1}{R} \frac{\partial \psi}{\partial R} = -\frac{2(R - R_0)}{R \delta R^2} \psi_0 e^{-t^2/\tau^2} \exp \left[-\frac{(R - R_0)^2}{\delta R^2} - \frac{Z^2}{\delta Z^2} \right]. \quad (4)$$

We also need to take into account the toroidal field, which is modelled using the vacuum expression $B_\varphi = B_0 R_0/R$ (where B_0 is a constant), and is assumed to be unaffected by the reconnection process.

It should be noted that the global poloidal field in the final, relaxed state of the plasma is not represented in this model. The fast ion orbits will of course be affected by this poloidal field, but it is not relevant to the acceleration process, which is the focus of our attention here. Once an ion has stopped accelerating, either because E_φ has dropped to a negligible level or because the ion has moved outside the acceleration region (due to grad- B , curvature or $\mathbf{E} \times \mathbf{B}$ drifts), we no longer need to track its orbit accurately. In any case the acceleration region lies close to the final location of the plasma magnetic axis, where, by definition, the poloidal field vanishes, and moreover the acceleration timescale ($\sim 1 \mu\text{s}$) is shorter than the timescales associated with motion in the toroidal and global poloidal fields (i.e. the bounce time for trapped ions and the toroidal transit time for circulating ions). For these reasons it is sufficient for our purposes to consider the fields associated with the reconnection process together with the toroidal magnetic field.

3.2 Test-particle simulations

The acceleration of test deuterons and protons was modelled using a full orbit-following code CUEBIT [10] for $20 \mu\text{s}$ from $t = 0$ (when $E_\varphi = 0$) in the fields described above, with $\tau = 1.5 \mu\text{s}$ and three different pairs of values of δR and δZ : (a) 0.1 m and 0.02 m; (b) 0.05 m and 0.01 m; (c) 0.025 m and 0.005 m. The implicit integration scheme used in CUEBIT guaranteed that energy changes could only occur through the action of E_φ rather than numerical effects. The parameter ψ_0 was chosen such that the maximum value of E_φ was 13 kV m^{-1} , slightly higher than the maximum electric field observed in the simulations of Stanier and co-workers [3]. The chosen values of δR and δZ are broadly consistent with the dimensions of the current sheets observed in these simulations and of the regions of strong electron heating measured experimentally by Tanabe and co-workers [1]. However it is appropriate to consider a range of values of these length scales since the detailed structure of the current sheet in the fluid simulations (although not the maximum electric field) was found to depend on the assumed value of a hyper-resistivity used in the generalized Ohm's law (see figure 7 in Ref [3]). In each simulation the orbits of 200,000 particles were tracked, and subsequently binned in energy to generate plots that could be compared directly with NPA energy spectra such as those shown in figure 2. We neglect collisional effects, for reasons that are discussed in the appendix.

Figure 6 shows the deuterium and hydrogen spectra obtained using the parameters listed above. In all three cases it can be seen that protons are accelerated to higher maximum energies than deuterons, consistent with both the experimentally-measured spectra shown in figure 2 and with simple estimates for particle acceleration in parallel electric fields. However only in cases (a) and (b) are the maximum energies close to the

measured values; in case (c), with the smallest current sheet, the maximum energies are clearly lower than the measured values. In the other two cases there is no difference in the maximum simulated particle energies, but case (b) seems to capture more of the features of the NPA deuterium data in that the spectrum for this species is less flat at low energy than in case (a), although it is still flatter than the measured spectrum. It is interesting to note that there is a break in the deuterium spectrum at about 10 keV in both the measurements and the synthetic spectra for cases (a) and (b). We conclude that the current sheet parameters that reproduce most accurately the measured spectra are $\delta R = 0.05$ m, $\delta Z = 0.01$ m.

Examination of individual particle orbits suggests that ions are accelerated to lower maximum energies in the case of the smallest assumed current sheet ($\delta R = 0.025$ m, $\delta Z = 0.005$ m) mainly because the magnetic field in the region of high E_φ is then mainly poloidal (since B_R and B_Z scale inversely with δZ^2 and δR^2 , respectively). This means that the parallel component of the electric field is significantly smaller than E_φ , and hence less effective at accelerating particles to high energies.

We can also infer fast ion pitch angle distributions from the CUEBIT simulations. Figure 7 shows the computed energy distributions of deuterons with v_φ/v in the range 0.97-1.00 (green curve) and in the range 0.94-0.97 (blue curve) at the end of the simulation with $\delta R = 0.1$ m, $\delta Z = 0.02$ m. In the energy range used here (chosen to provide an exact comparison to the NPA data), a negligible number of ions had $v_\varphi/v < 0.94$. It is evident from figure 7 that the accelerated deuterons in the simulation had a pitch distribution that was very strongly peaked in the toroidal direction, particularly at high energy. By this stage of this simulation the poloidal field associated with the reconnection process had decayed to a negligible level, and so the toroidal direction coincided with the direction of \mathbf{B} . As shown in section 2, the NPA measurements in shots with different R_{NPA} imply strong field-aligned anisotropy in the fast ions during merging, and the CUEBIT simulations are qualitatively consistent with the experimental data in this respect. Figure 3 suggests that the true fast ion anisotropy is less extreme than that indicated by the simulations; this could be due in part to the neglect of the global poloidal field in the simulations.

4 Modelling of microwave emission

Microwave bursts similar to those described in section 2 were detected during the early stages of edge localised modes (ELMs) in MAST, and attributed to the anomalous Doppler instability (ADI), driven by strongly field-aligned energetic electron distributions resulting from parallel electric fields [11]. However, unlike the bursts observed during merging start-up, those correlated with ELMs were often accompanied by strong enhancements (up to a factor of two or more) in soft X-ray emission, providing clear evidence of energetic electrons with energies exceeding the soft X-ray threshold of about 1 keV. However the non-detection of soft X-ray emission enhancements during the early stages of merging does not necessarily preclude the presence of suprathermal electrons at that time, for two reasons. First, the pre-merging electron temperature was about 10 eV, i.e. about two orders of magnitude below the soft X-ray threshold, and therefore

1
2
3
4
5
6
7 a suprathermal electron population with energies in the range 10 eV - 1 keV could not
8 have been detected using the soft X-ray diagnostic. Second, the bulk density in the
9 plasma core region was generally about an order of magnitude lower during the merging
10 phase than in the flat-top phase, and the emissivity of nonthermal bremsstrahlung is
11 proportional to the densities of both the nonthermal electrons and the bulk ions which
12 are decelerating them. Typically the soft X-ray signals recorded prior to the merging
13 phase are very noisy, and it is possible that the bremsstrahlung signature of a dilute
14 suprathermal electron population could remain within the noise, even if some of these
15 electrons have energies in excess of the X-ray energy threshold.
16
17

18 With these considerations in mind, we have used a one-dimensional particle-in-cell
19 (PIC) code EPOCH [12] to model an equilibrium plasma containing bulk electrons and
20 ions with temperature 10 eV, density $2.5 \times 10^{18} \text{ m}^{-3}$ and a dilute (1% concentration)
21 magnetic field-aligned electron beam with a flat velocity distribution extending to a
22 maximum energy of 1.6 keV (our reasons for choosing this particular value are explained
23 below). The magnetic field was set equal to 0.82 T, corresponding to the toroidal field
24 at the major radius of peak electron heating during the merging phase of MAST pulse
25 28146 (cf. figure 4). The field was tilted at an angle α of 65° with respect to the single
26 space direction to accommodate waves with $k_{\parallel}, k_{\perp} \neq 0$.
27
28

29 Figure 8 is a logarithmic plot of the longitudinal (i.e. parallel to the wave vector)
30 electric field amplitude in wave number/frequency space, obtained by Fourier analysing
31 the simulation results corresponding to a period between 832 and 999 electron cyclotron
32 periods after $t = 0$. The dominant feature in this dispersion plot is a strong mode at
33 about 5 GHz, below the SAMI frequency range; a somewhat weaker mode appears at
34 a frequency of about 26 GHz, close to the peak microwave burst frequency (~ 26.5 GHz)
35 in MAST pulse 28146 (see figure 4). While figure 8 shows the electrostatic compo-
36 nent of the fluctuations, lower amplitude excitation is also visible in the electric field
37 component perpendicular to both the wave vector and the magnetic field, indicating
38 that the fluctuations have an electromagnetic component. This is important in terms
39 of diagnostic interpretation, since, in order to be detected by SAMI, a plasma wave
40 mode must either have an electromagnetic component or acquire one through a mode
41 conversion process.
42
43
44

45 It is instructive to compare the results shown in figure 8 with the following expression
46 for the frequencies of electrostatic modes in a cold magnetised plasma [13]:
47
48

$$49 \nu_{1,2}^2 = \frac{1}{2} \nu_{\text{UH}}^2 \pm \frac{1}{2} \left[\nu_{\text{UH}}^4 - 4\nu_{ce}^2 \nu_{pe}^2 \cos^2 \alpha \right]^{1/2}. \quad (5)$$

50
51 Evaluating these frequencies using the equilibrium density and magnetic field of the
52 EPOCH simulation, we obtain $\nu_1 \simeq 5$ GHz, $\nu_2 \simeq 26$ GHz, which match closely the fre-
53 quencies of the two modes apparent in figure 8. The higher of these two frequencies is
54 very close to the upper hybrid frequency ν_{UH} . As in the case of the PIC simulations
55 reported in Ref [11], it appears that these normal modes are being excited due to the
56 anisotropy in the fast electron tail via the anomalous Doppler resonance condition
57
58
59

$$60 \omega - k_{\parallel} v_{\parallel} - \ell \Omega_e = 0, \quad (6)$$

where $\ell = -1$, ω is the angular wave frequency, $\Omega_e = 2\pi\nu_{ce}$ and $k_{\parallel}, v_{\parallel}$ denote wavenum-

ber and electron velocity components parallel to \mathbf{B} . At resonance we thus have

$$\frac{\omega}{k_{\parallel}} = \frac{\omega}{\omega + \Omega_e} v_{\parallel}. \quad (7)$$

To avoid strong Landau damping on the bulk electron population, ω/k_{\parallel} needs to be at least several times the electron thermal speed. This constraint, combined with (7), means that there is a minimum suprathermal tail velocity for the anomalous Doppler instability to be excited, which determined the choice of maximum electron tail energy (1.6 keV) in the simulation. This maximum energy is comparable to the low energy threshold of the soft X-ray detectors in MAST (~ 1 keV), and, as we noted in section 2, the relatively low densities of MAST plasmas during the early merging phase means that the presence of suprathermal electrons with energies above this threshold cannot in any case be ruled out. On this basis we conclude that the the anomalous Doppler instability, excited by anisotropic suprathermal electrons, provides a possible explanation of the microwave burst shown in figure 4.

As shown in figure 5, the highest intensity microwave bursts during merging in MAST ranged in frequency from 10 GHz to 30.5 GHz (although in individual bursts the emission was generally narrow-band, as shown in figure 4). It is not certain that the anomalous Doppler instability can account for the full range of measured burst frequencies, although it should be noted that there was some variation in the major radius (which determined ν_{ce}) at which peak electron heating occurred during merging, and the electron density at this location (which determined ν_{pe}) also had a range of values. Moreover the frequencies excited by the anomalous Doppler instability also depend on the propagation angle α of the wave with respect to \mathbf{B} , and it is not possible to determine values of this parameter from the available data. While it is unclear whether all of the microwave bursts detected during merging in MAST can be attributed specifically to the anomalous Doppler instability, the high intensities, short durations and narrow bandwidths of these bursts suggest strongly they were all caused by the presence of suprathermal electrons.

5 Conclusions and discussion

We have demonstrated that MAST neutral particle analyser (NPA) and microwave data provide strong evidence of, respectively, ion and electron acceleration due to magnetic reconnection associated with merging plasma start-up. Ion energy spectra from pulses with different NPA lines-of-sight suggest that the fast ions are strongly aligned with the magnetic field. Modelling of ion acceleration, using axisymmetric fields obtained from an assumed time-varying poloidal flux based on Hall-MHD simulations of the reconnection process, has yielded results that reproduce some of the features of the NPA data, for example the inferred strong field alignment of the fast ion distributions and the result that protons are accelerated to higher energies than deuterons. A particle-in-cell (PIC) simulation of a plasma with a magnetic field-aligned suprathermal electron population, and bulk parameters approximating those of the merging phase in a particular MAST pulse, shows the excitation of waves via the anomalous Doppler instability

(ADI) at a frequency close to that of a high intensity microwave burst detected during this pulse. The ADI thus provides a credible explanation of this particular burst, although the absence of simultaneous enhancements in soft X-ray emission suggests that few of the fast electrons were accelerated to energies higher than about 1 keV.

In reality plasma merging in MAST is likely to have been to some extent a three-dimensional process, and so the ion modelling presented in section 3 could in principle be made more realistic by adding φ -dependent terms to the reconnecting flux, ψ . However $E_\varphi = -(1/R)\partial\psi/\partial t$ would then also depend on φ , and it would thus be necessary to include additional components in the electric field to ensure that it remained divergence free, as required by quasineutrality. It would not therefore be straightforward to extend the model in this way. Nevertheless three-dimensional effects may need to be considered since, in the framework of the two-dimensional model and the very large electric fields occurring in the Hall-MHD simulations reported in Ref [3], it is difficult to account for the fact that there is no evidence for electron runaway acceleration during merging. The collision time of a bulk electron prior to merging is much shorter than that of a bulk ion (for the parameters used in the PIC simulation it is about $0.2 \mu\text{s}$), but collisions would not prevent runaway acceleration from occurring when super-Dreicer electric fields are present, as suggested by the fluid simulations.

An alternative possibility is that electrons are transported away from the acceleration region too rapidly to undergo runaway acceleration due to three-dimensional field perturbations. It is well-established that stochastic magnetic fields produce a cross-field particle diffusivity D_{RR} given by [14]

$$D_{\text{RR}} \sim v_{\parallel} L_B \left(\frac{\delta B}{B} \right)^2, \quad (8)$$

where L_B is the parallel length scale of the magnetic field and δB is the typical fluctuation in the field. If we assume that vertical transport due to this effect is as likely to occur as radial transport, the confinement time τ_c of particles in the acceleration region is then determined principally by δZ , since we have taken this to be smaller than δR :

$$\tau_c = \frac{\delta Z^2}{D_{\text{RR}}} = \frac{\delta Z^2}{v_{\parallel} L_B} \left(\frac{B}{\delta B} \right)^2. \quad (9)$$

A particle of mass m will not undergo significant further acceleration if $\tau_{\text{acc}} \equiv mv_{\parallel}/eE_{\parallel} > \tau_c$. Using (9), we deduce that this inequality leads to the following expression for the magnetic field fluctuation level required to quench the acceleration process:

$$\frac{\delta B}{B} > \left(\frac{\delta B}{B} \right)_{\text{crit}} \equiv \left(\frac{\delta Z^2 e E_{\parallel}}{2 \mathcal{E} L_B} \right)^{1/2}, \quad (10)$$

where $\mathcal{E} = mv_{\parallel}^2/2$ is the particle's parallel kinetic energy. For a given fluctuation level, (10) implies the same maximum energy for particles of different mass. The ions recorded in figure 2 had energies of up to about 20 keV. With $L_B \sim 2\pi R$, $E_{\parallel} = 10 \text{ kV m}^{-1}$ and $\delta Z = 0.01 \text{ m}$, it follows from (10) that particles with this energy would typically be ejected from the reconnecting current sheet before undergoing significant further acceleration if $\delta B/B \sim 2 \times 10^{-3}$ (note however that the ion energies in our particle simulations were not limited by three-dimensional perturbations, since a two-dimensional

1
2
3
4
5
6
7 model was used in these simulations). It is reasonable to suppose that field fluctua-
8 tions of this magnitude could occur during the merging process, given that it resulted
9 in a sudden transformation of the magnetic field topology of the plasma and a very
10 rapid increase in its thermal energy [1]. In such a scenario electrons would be expected
11 to have about the same maximum energy as ions, i.e. ~ 20 keV. As noted previously,
12 there is no evidence from soft X-ray data for the presence during the early merging
13 phase of suprathermal electrons with energies higher than about 1 keV, although this
14 could be due to the nonthermal bremsstrahlung emissivity being below the detection
15 threshold, given the low densities of MAST plasmas during this phase. In any event
16 three-dimensional field perturbations provide a possible explanation of the fact that
17 runaway electron acceleration did not occur during merging in MAST, despite the
18 presence of electric fields capable of accelerating ions to energies in the tens of keV
19 range.
20
21
22

23 Fast ion and electron production during merging start-up in MAST does not appear
24 to have had any adverse consequences for plasma performance during the flat-top phase.
25 The significance of the results presented in this paper lies chiefly in the insights they
26 provide into the basic plasma physics of reconnection-induced particle acceleration.
27 In solar flares, fast electrons with energies in the tens and hundreds of keV range
28 can be detected much more readily (via hard X-ray and microwave emission) than
29 fast ions with energies in the same range [5]. During merging-compression in MAST,
30 the situation is reversed, insofar as substantial fluxes of suprathermal ions have been
31 detected directly via charge-exchange with neutrals whereas we have only indirect
32 evidence (in the form of microwave bursts) for the presence of suprathermal electrons.
33 The results from MAST thus suggest that parallel electric fields arising from magnetic
34 reconnection can be at least as effective in producing fast ions as fast electrons, and,
35 given the similarity noted previously between plasma conditions during merging in
36 MAST and those in the flaring solar corona, it is reasonable to conjecture that this
37 may also be the case in solar flares.
38
39
40
41
42

43 Acknowledgments

44
45 The authors are grateful to Luca Garzotti (CCFE) and Hiroshi Tanabe (University
46 of Tokyo) for helpful discussions on soft X-ray measurements and the interpretation
47 thereof during merging in MAST. This work has received funding from the RCUK
48 Energy Programme [grant number EP/P012450/1]. SCC acknowledges a Fulbright-
49 Lloyds of London Scholarship and AFOSR grant no FA9550-17-1-0054. To obtain
50 further information on the data and models underlying this paper please contact Pub-
51 licationsManager@ukaea.uk.
52
53
54

55 Appendix. Ion collisions

56
57 For the purposes of computing ion orbits in the fields described in section 3 we neglect
58 collisions. For a bulk ion of mass m_i and charge Ze colliding with ions of the same
59
60

species with temperature T_i and density n_i , the collision rate is given by [2]

$$\nu_{ii} = \frac{2^{1/2}}{12\pi^{3/2}} \frac{n_i Z^4 e^4 \ln \Lambda}{m_i^{1/2} T_i^{3/2} \epsilon_0^2}, \quad (\text{A.1})$$

where $\ln \Lambda$ is the appropriate Coulomb logarithm and ϵ_0 is the permittivity of free space. Thomson scattering measurements at the start of the merging process in MAST pulse 9153 indicate values of electron density and temperature of around $n_e \simeq 10^{19} \text{ m}^{-3}$ and $T_e \simeq 30 \text{ eV}$ in the vicinity of the merging point. If we make the reasonable assumptions that $n_i \simeq n_e$ and $T_i \simeq T_e$ in the highly collisional pre-merging plasma, we infer from (A.1) an ion-ion collision time of about $26 \mu\text{s}$. Since this is much longer than the duration ($\sim 1 \mu\text{s}$) of large reconnection-induced parallel electric fields in the simulations of Stanier and co-workers [3], we are justified in neglecting ion-ion collisions in our particle simulations.

We also need to consider the possibility that collisions of test ions with bulk electrons could affect the acceleration process, since, in the usual case in which the ions are moving slower than the electrons, the ion-electron collision rate ν_{ie} is a constant, and therefore the corresponding drag force increases with the test ion speed, potentially setting a limit to the energy gain. This can be seen from the equation of motion

$$m_i \frac{dv_{\parallel i}}{dt} = ZeE_{\parallel} - m_i \nu_{ie} v_{\parallel i}, \quad (\text{A.2})$$

where $v_{\parallel i}$, E_{\parallel} denote the components of the test ion velocity and electric field parallel to \mathbf{B} . Acceleration will evidently cease if $v_{\parallel i}$ reaches a value $v_{\max} = ZeE_{\parallel}/m_i \nu_{ie}$. For $v_{\parallel i}$ less than the electron thermal speed v_e , we have [2]

$$\nu_{ie} = \frac{2^{1/2}}{12\pi^{3/2}} \frac{n_i Z^2 e^4 m_e^{1/2} \ln \Lambda}{m_i T_e^{3/2} \epsilon_0^2}, \quad (\text{A.3})$$

This expression for ν_{ie} , evaluated with the same bulk plasma parameters as before ($n_i = 10^{19} \text{ m}^{-3}$, $T_e = 30 \text{ eV}$), together with $E_{\parallel} = 10 \text{ kV m}^{-1}$, implies a value of v_{\max} which is much higher than v_e , indicating that (A.3) is not in fact applicable, and therefore that the ion-electron collisional drag force does not in this case limit the energy gain. In any case 10 kV m^{-1} is much higher than the Dreicer field for typical densities and temperatures in MAST prior to plasma merging. It may be concluded that the ion acceleration process can be modelled without needing to take into account either ion-ion or ion-electron collisions.

References

- [1] Tanabe H *et al* 2015 *Phys. Rev. Lett.* **115** 215004
- [2] Helander P and Sigmar D J 2002 *Collisional Transport in Magnetized Plasmas* (Cambridge: Cambridge University Press)
- [3] Stanier A, Browning P, Gordovskyy M, McClements K G, Gryaznevich M P and Lukin V S 2013 *Phys. Plasmas* **20** 122302

- 1
2
3
4
5
6
7 [4] Helander P, Eriksson L-G, Akers R J, Byrom C, Gimblett C G and Tournianski
8 M R 2002 *Phys. Rev. Lett.* **89** 235002
9
- 10 [5] McClements K G and Turnyanskiy M R 2017 *Plasma Phys. Control. Fusion* **59**
11 014012
12
- 13 [6] Emslie A G, Miller J A and Brown J C 2004 *Astrophys. J.* **602** L69
14
- 15 [7] Tournianski M R, Carolan P G and Akers R J 2004 *Rev. Sci. Instrum.* **75** 2854
16
- 17 [8] Turnyanskiy M R, Keeling D L, Akers R J, Cunningham J G, Conway N J, Meyer
18 H, Michael C A and Pinches S D 2009 *Nucl. Fusion* **49** 065002
19
- 20 [9] Shevchenko V F, Vann R G L, Freethy S J and Huang B K 2012 *J. Instrumentation*
21 **7** P10016
22
- 23 [10] Hamilton B, McClements K G, Fletcher L and Thyagaraja A 2003 *Sol. Phys.* **214**
24 339
25
- 26 [11] Freethy S J, McClements K G, Chapman S C, Dendy R O, Lai W N, Pamela S J
27 P, Shevchenko V F and Vann R G L 2015 *Phys. Rev. Lett.* **114** 125004
28
- 29 [12] Lai W N, Chapman S C and Dendy R O 2015 *Phys. Plasmas* **22** 112119
30
- 31 [13] Mikhailovskii A B 1974 *Theory of Plasma Instabilities, Vol 1: Instabilities of a*
32 *Homogeneous Plasma* (New York: Consultants Bureau)
33
- 34 [14] Rechester A B and Rosenbluth M N 1978 *Phys. Rev. Lett.* **40** 38
35
36
37
38
39
40
41
42
43
44
45
46
47
48
49
50
51
52
53
54
55
56
57
58
59
60

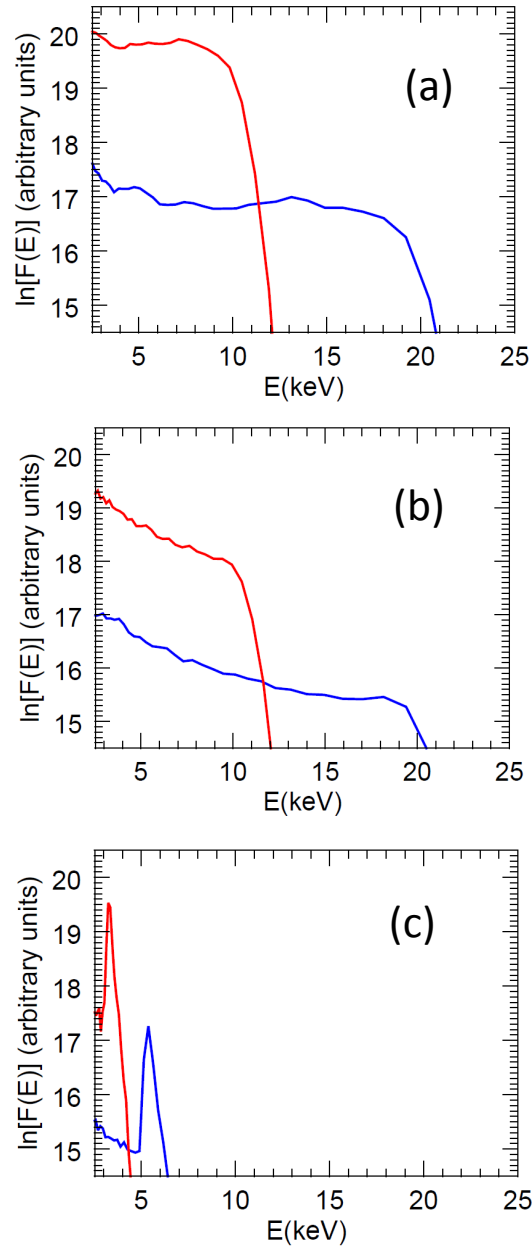


Figure 6: Deuterium (red) and hydrogen (blue) energy spectra obtained using CUEBIT with (a) $\delta R = 0.1$ m, $\delta Z = 0.02$ m, (b) $\delta R = 0.05$ m, $\delta Z = 0.01$ m and (c) $\delta R = 0.025$ m, $\delta Z = 0.005$ m.

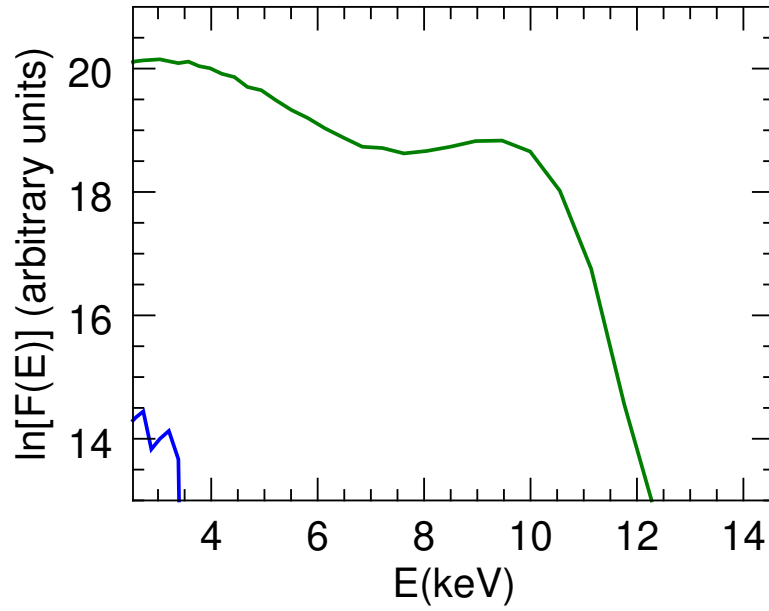


Figure 7: Energy distributions of deuterons with pitch v_ϕ/v in the range 0.97-1.0 (green curve) and 0.94-0.97 (blue curve) in CUEBIT simulation with $\delta R = 0.1$ m, $\delta Z = 0.02$ m.

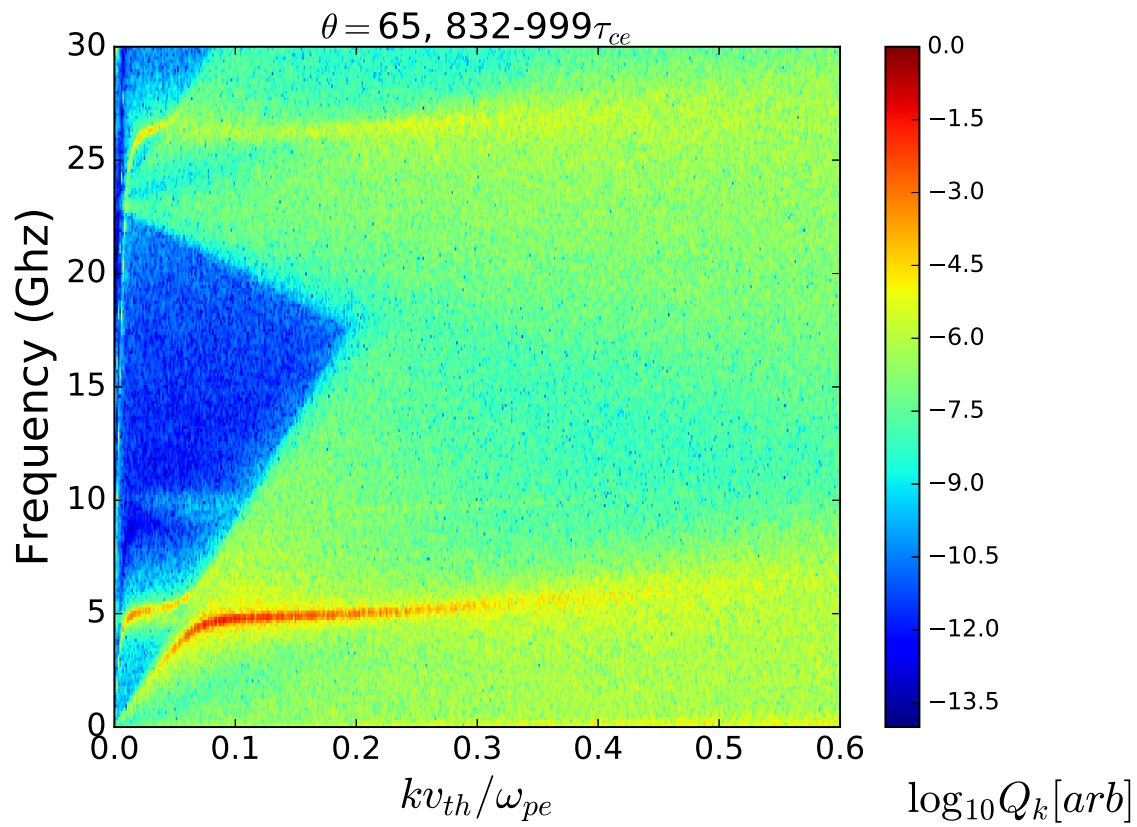


Figure 8: Electrostatic field amplitude versus wave number and frequency in EPOCH simulation with bulk plasma parameters characteristic of merging plasmas in MAST and a dilute suprathermal electron beam.